A First-Principles DFT Study of UN Bulk and (001) Surface: Comparative LCAO and PW Calculations

R. A. EVARESTOV,[1] A. V. BANDURA,[1] M. V. LOSEV,[1] E. A. KOTOMIN,[2] Yu. F. ZHUKOVSKII,[2] D. BOCHAROV[2]
[1]*Department of Quantum Chemistry, St. Petersburg State University, 198504 St. Peterhof, University Prospect 26, Russia*
[2]*Institute for Solid State Physics, University of Latvia, 8 Kengaraga Str., Riga, LV-1063, Latvia*

Received 13 January 2008; Revised 10 April 2008; Accepted 11 April 2008
DOI 10.1002/jcc.21023
Published online 21 May 2008 in Wiley InterScience (www.interscience.wiley.com).

Abstract: LCAO and PW DFT calculations of the lattice constant, bulk modulus, cohesive energy, charge distribution, band structure, and DOS for UN single crystal are analyzed. It is demonstrated that a choice of the uranium atom relativistic effective core potentials considerably affects the band structure and magnetic structure at low temperatures. All calculations indicate mixed metallic-covalent chemical bonding in UN crystal with U5*f* states near the Fermi level. On the basis of the experience accumulated in UN bulk simulations, we compare the atomic and electronic structure as well as the formation energy for UN(001) surface calculated on slabs of different thickness using both DFT approaches.

 J Comput Chem 29: 2079–2087, 2008

Key words: first-principles calculations; actinides; uranium nitride

Introduction

Uranium mononitride and carbide (UN, UC) attract a considerable attention as promising nuclear fuel materials for novel Generation IV reactors.[1] In particular, nitrides and carbides exhibit higher thermal conductivity, melting temperature, and metal density when compared with uranium dioxide that is commonly used nowadays. To predict nuclear fuel performance under different operating conditions and then a prolonged time in repository for used fuel, it is necessary to understand and predict material physicochemical properties. Of special importance are surface properties because commercial fuels are used as powders and UN, UC are effectively oxidized in air. The more so, numerous grain boundaries considerably affect material properties.

Theoretical studies of uranium compounds are difficult due to a relativistic character of electron motion in the U atom core and strong electron–electron correlation. Moreover, UN is a rather complicated system because it is characterized by a mixed metal-covalent chemical bonding. The metallic part (U5*f* states near the Fermi level) is better described by a delocalized basis of the Plane Waves (PW), whereas the covalent part (U5*f*-N2*p* hybridization) by a Linear Combination of Atomic Orbital (LCAO) basis set. This is why in this article we compare results of both approaches.

In Section "Previous *ab initio* simulations on UN bulk," the comparison is made for the bulk properties (studied earlier experimentally), with a detailed analysis of relativistic pseudopotentials in Section "Current DFT LCAO and PW calculations on UN bulk." In "DFT LCAO and PW calculations on UN(001) surface" section, we discuss—for the first time—the (001) surface properties (so far, the atomistic simulations on U compound substrates were performed only for densely packed UO_2 surfaces[2]).

Previous *Ab Initio* Simulations on UN Bulk

UN single crystal possesses *fcc* (face-centered cubic) structure with two atoms per unit cell: the lattice constant $a_0 = 4.886$ Å, the bulk modulus $B = 194$ GPa, and the cohesive energy $E_0 = 13.6$ eV.[1] These properties could be used as the test for theoretical calculations. Below 53 K UN undergoes the antiferromagnetic (AFM) ordering with the doubled unit cell and the spin density (SD) of 0.75 μ_B per U ion (at 4.2 K). Above this temperature, it reveals paramagnetic properties with the effective magnetic moment in the Curie-Weiss law of $\sim$3.1 μ_B. UN shows a metallic conductivity.

So far, most of calculations were performed for the high temperature phase (a primitive unit cell) relevant for fuel applications. The first relativistic KKR[3] and LMTO[4] calculations were performed already in 80s focusing mostly on the atomic and band structure of UN crystal. The calculated lattice parameters were within 3% of the experimental value, whereas the bulk

Correspondence to: R. A. Evarestov; e-mail: re1973@re1973.spb.edu

Table 1. Calculated Properties of UN Bulk Crystal.[a]

Property	PBE-AE-LAPW[5,6 b]	PBE-US[9]	PW91-PAW[10 c]	PW91-US[11 d]	PW91-AE[12]	PW91-LCAO[13 e]
a_0, Å	4.886	4.820	4.864	4.954	4.90	Fixed expt.
B, GPa	209		226	182		
E_c, eV	13.4		14.7	12.3		9.9–12.8
SD, μ_B	1.25		1.05			3.02–3.20

Lattice constant a_0, bulk modulus B, cohesive energy E_c and spin density SD per unit cell. AE, all electrons; US, ultrasoft pseudopotentials.
[a]In the LCAO approach, the value of E_c is calculated with respect to the free N and U atoms, whereas in the PW approach it was estimated with respect to the same atoms placed in cubic supercells with large (10 Å) translation vectors.
[b]WIEN-2k code.
[c]VASP code.
[d]CASTEP code.
[e]GAUSSIAN code.

modulus was reproduced worse, within 11%. Only recently these first principles calculations were continued (Table 1). In particular, the all-electron (AE) LAPW calculations (refs. 5, 6; Sedmidubsky et al., unpublished, 2005) were performed using the GGA-PBE (Perdew-Burke-Ernzerhof) exchange correlation functionals with and without incorporation of the spin-orbital interaction (WIEN-2k computer code) for a series of actinide nitrides. The calculated cohesive energy and the lattice constant are close to the experimental values. Incorporation of the spin-orbital coupling leads to a large (8.2 eV) splitting of U*6p* semicore into $6p_{1/2}$ and $6p_{3/2}$ as well as slight reduction of the magnetic moment from 1.25 down to 1.16 μ_B. The hybridization of N*2p*, U*5f*, and U*6d* states was observed in the Brillouin zone (BZ) due to their overlap: the N*2p* energy levels lie in the region of -6 to -1 eV whereas the U*5f* states dominate near and at the Fermi level. The calculated band structure around the Fermi level is in qualitative agreement with the experimental UPS spectra.[7,8]

In ref. 6 the WIEN-2k calculations were complemented by a study of the AFM phase. The lattice constant is in a good agreement with the experiment (~0.4%), but—unlike the experiment—the ferromagnetic structure is found to be lower in energy, with the SD = 0.96 μ_B. It should be pointed out that this is presumably a failing of the PBE functional. Notice, that due to use of muffin-tin spheres, the attribution of the electronic and spin density to individual ions is not uniquely defined.

Systematic DFT-PW calculations were also performed, starting with a study[9] focused on the UN and UC atomic structure. Using the ultra-soft (US) pseudopotentials and PBE96 exchange-correlation functional, the experimental UN and U_2N_3 lattice constants were reproduced within 3% error. In the more detailed UN, UN_2, and U_2N_3 DFT PW calculations, the VASP[10] and CASTEP[11] codes using the Perdew-Wang (PW91) nonlocal GGA exchange-correlation functional[14] were employed and combined with either the US or PAW pseudopotentials, respectively. Both methods agree on complicated mixed metallic-covalent nature of the UN chemical bonding and reproduce well the lattice constants, bulk moduli, and cohesive energies. Analogously to previous calculations for the primitive unit cell, they suggest the magnetic moment on U ion close to unity. The DFT PW approach combined with a supercell model was further used in the calculations of defective UN crystal, containing single point defects and Frenkel and Schottky defect pairs.[10,11] A study of defect properties is of key importance for the prediction of fuel behavior under operational conditions and in further centuries-long depository.

One more first-principles all-electron relativistic DFT study with GGA PW91 exchange correlation functional and numerical double ξ basis set was performed recently for UN and UN_2[12]; the results are compared with the experimental EXAFS and X-ray diffraction data. New element in that article is a calculation of the phonon frequencies and heat capacities, which are important for the fuel behavior prediction. Authors provide additional evidence for an important role of itinerant U*5f* states in thermodynamic properties.

To understand better the UN fuel performance, careful study of the chemical bonding in crystalline bulk and its surface properties is a necessary step. The LCAO approach is a natural way for such a study as it extends for the periodic systems the chemical bonding analysis developed in quantum chemistry of molecules,[15] and it is free of muffin-tin approximation problems. In particular, recent first principles DFT and hybrid HF-DFT LCAO calculations of UO_2 crystal[16] provided the structural, electronic, and magnetic properties in a good agreement with the experimental data.

The ground state valence electronic configurations of U and N atoms are $5f^3 6d^1 7s^2$ and $2s^2 2p^3$, respectively. In a crude ionic bonding picture, the U*6d* and *7s* electrons fill the N*2p* states and the three U*5f* electrons form the highest occupied molecular orbital (HOMO).[17] The LCAO calculations allow one to study this qualitative picture in more detail, analyzing the changes of the free atom electronic structure due to the chemical bonding formation, and to connect the energy bands of a solid with the atomic states. However, the first LCAO electronic structure calculations of crystalline UN have been only recently performed.[13] In that article, several different Relativistic Effective Core Potentials (RECP) containing 60, 78, and 81 electrons in a U ion core, which are discussed in more detail in the next RECP Formalism, were used and compared. In particular, for the RECP78, there exist 14 outermost uranium atom electrons

included into the valence shell ($6s^26p^66d^15f^37s^2$). The results obtained were compared with those for RECP60, where 32 outermost uranium atom electrons are included in the valence shell (the configuration $5s^25p^65d^{10}6s^26p^66d^15f^37s^2$). Lastly, in the RECP81 U5*f* electrons are included into the atomic core.

Recent LCAO calculations on UN bulk[13] have been performed using the GAUSSIAN-03 computer code with the PW91 exchange-correlation functional and periodic boundary conditions. Unlike previous PW calculations, the LCAO (RECP78) suggests the ground state with the three unpaired electrons ($S_z = 3/2$, i.e., $SD \approx 3\ \mu_B$) whereas the $S_z = 1/2$ state lies slightly higher in energy (~0.5 eV). The latter is close to that experimentally observed. The values of cohesive energy calculated for RECP78 and RECP60 considerably differ (9.86 and 12.8 eV, respectively, last column in Table 1), thus indicating an importance of the U outer shell relaxation.

Group-theoretical analysis performed for interpretation of the UN band structure demonstrates that threefold degenerate (at Γ point) U5*f* t_{2u} state is split at X and W points of the BZ due to hybridization with the N2*p* states, which produces a narrow band near the Fermi level (~2 eV). This band is occupied with 3 spin-up electrons. The U5*f* t_{1u} state is allowed by symmetry to mix up with N2*p* state at the Γ point and form a broad band to the lower-energy side. Lastly, the nondegenerate U5*f* a_{2u} state is empty; it forms the bottom of the conduction band (CB). In other words, both bottom of the CB and the top of the valence band (VB) are formed by U5*f* states which leads to the metallic nature of this compound[13] (unlike UO_2 which is a semiconductor[16]). The Mulliken effective atomic charges of ±(1.5–2.0) *e* calculated using the GAUSSIAN-03 code confirm the mixed nature of the UN chemical bonding and are in agreement with the Bader topological charges of ±1.6 *e* obtained in PW calculations.[11]

Current DFT LCAO and PW Calculations on UN Bulk

RECP Formalism

As mentioned above, the proper choice of relativistic core pseudopotentials is important for reliable DFT calculations. The different methods for construction of RECP have been suggested so far.[15] To the best of our knowledge, the small core (SC) pseudopotentials of U atom (60 core electrons, with 5*s*, 5*p*, and 5*d* electrons referred to the valence shell) were generated only for LCAO calculations. Unreliability of the large core (LC) pseudopotentials RECP78 for U was known in calculations of uranyl UO_2^{+2} ion[18] as well as molecules of uranium fluorides UF_5 and UF_6.[19] In particular, the most famous molecular failure was that for the uranyl ion, predicted to be bent using the LC RECP, whereas the correct linear structure was recovered only with the SC pseudopotential.

We use here the energy-adjusted small core (SC) pseudopotential by Stuttgart-Cologne group (SC60).[20] Its parameters are fitted to the excitation and ionization energies obtained in the relativistic all-electron calculations performed using a numerical finite difference approach. The RECP generation method based on numerical Dirac-Hartree-Fock wave function, allows one the computation of averaged (over $(l-1/2)$ and $(l+1/2)$ components) relativistic effective potentials (AREP) and includes also the effective spin-orbit potential (ESOP) operators. Use of the energy-adjusted pseudopotentials SC60 in the complete form (with ESOP) requires use of a two-component spinor (spin-orbital) formalism in molecular or crystalline calculations. In our scalar-relativistic calculations only the AREP part of RECP has been employed.

The accuracy of the calculations with the energy-adjusted RECPs is essentially limited by the demand that only the radially local (semilocal) RECP operator is used. A more strict treatment of the outermost core electrons (for example, U6*s* and 6*p* electrons) demands to treat them explicitly. Since effective potentials are somewhat different for the outermost core and valence electrons with the same orbital and total moment, new terms with projectors on the outermost core pseudoorbitals were added to the conventional core pseudopotential operator in the Generalized RECP (GRECP) method (see ref. 21 and references herein). The importance of additional nonlocal terms in the expression GRECP operator is demonstrated in U atom calculations.[22] In the present calculations we have used for U atom the only radially local AREP version by the Mosyagin-Titov LC (MT78) and SC (MT60) pseudopotentials.[13]

The radially local AREP form used in LCAO calculations is a sum of a Coulomb term *C*, a local term V_{loc} and a semilocal term V_{sl} usually presented analytically as

$$V_{PS}(\mathbf{r}) = C + V_{loc} + V_{sl} = -\frac{Z_N}{r} + \sum_{k=1}^{M} r^{n_k-2} C_k \exp(-\alpha_k r^2) + \sum_{l=0}^{3}\left[\sum_{k=1}^{M_l} r^{n_{kl}-2} C_{kl} \exp(-\alpha_{kl} r^2)\right]\hat{P}_l \quad (1)$$

where Z_N in a Coulomb term is the effective nuclear charge (total nuclear charge minus the number of electrons represented by RECP); n_k, n_{kl} = 0, 1, 2 and C_k, C_{kl}, α_k, α_{kl} are fitting parameters. The local term is a sum of products of polynomial and Gaussian radial functions whereas a semilocal term contains a sum of products of polynomial radial functions, Gaussian radial functions and angular momentum projection operators $\hat{P}_l$. Therefore, to specify the semilocal RECP, one needs to include a set of triplets (coefficient, power of *r* and exponent) for each term in each angular momentum of RECP. The contraction coefficients C_k, C_{kl}, exponents α_k, α_{kl} and powers n_k, n_{kl} are found by fitting the numerical AREP to expansions in Gaussian type functions (GTF) for the different RECP versions.

For each AREP the corresponding numerical atomic orbitals are approximated by the GTFs linear combinations, including both contracted and primitive GTOs. In particular, the contracted part of a U basis set (12*s*11*p*10*d*8*f*)/(8*s*7*p*6*d*4*f*) corresponding to the RECP SC60 in the segmented contraction scheme, defines three *s*-type (5*s*, 6*s*, 7*s*), two *p*-type (5*p*, 6*p*), two *d*-type (5*d*, 6*d*) and one *f*-type (5*f*) orbitals, occupied by the valence electrons in the ground state of U atom. The rest (primitive) GTOs are polarizing and diffuse orbitals necessary to properly describe the tails of the free-atom wave functions. The basis sets 11*s*5*p*6*d*5*f* and 6*s*3*p*4*d*4*f* have been used in our MT60 and MT78 RECP calculations, respectively. Table 2 presents the diffuse primitive Gaus-

Table 2. Diffuse Primitive Gaussian Exponents in the Basis Set of a Free U Atom Corresponding to the Stuttgart-Cologne Pseudopotential SC60.[18]

	Shell type			
GTO	*s*	*p*	*d*	*f*
1	0.071170	0.005000	0.073273	0.181420
2	0.030539		0.005000	0.005000
3	0.005000			

sian exponents in the basis set of a free U atom corresponding to the SC60 pseudopotential.

It is well known that for LCAO bulk calculations the basis set (BS) of free atom has to be modified as the diffuse functions cause numerical problems because of the large overlap with the core functions of the neighboring atoms in a dense-packed crystal.[15] This is why in the bulk calculations the diffuse exponents are either removed (as done in our calculations) or optimized, in order to minimize the total energy per unit cell. For example, the detailed BS optimization performed for Hartree-Fock (HF) and DFT LCAO calculations on $ATiO_3$ perovskites (A = Sr, Ba, Pb)[15] resulted in a good correlation with available experimental data (lattice parameters, bulk moduli and optical band gaps). Although there exist different algorithms for minimization of many-variables functions,[23,24] no analysis of their efficiency for the BS optimization in crystals was done so far.

In our PW calculations presented here the VASP code[25] was applied with the projector-augmented-wave (PAW) pseudopotentials for U and N atoms. The PAW method by Blöchl[26] uses the transformation operator between pseudo-orbitals and original orbitals combining the pseudopotential approach and LAPW method. The U PAW78 pseudopotential with a large U core (LC) RECP (78 core electrons, 14 valence electrons) is the same as in previous VASP calculations on UN[10,11] containing the closed shell configuration $6s^26p^65f^26d^27s^2$ while the U ground state possesses an open shell configuration known as $6s^26p^65f^36d^17s^2$.[25] Unlike those calculations, we have used here two different exchange-correlation functionals and very high accuracy in both *k*-point mesh and cut-off energy. Both LCAO and PW spin-polarized (FM) bulk calculations have been performed for the cubic crystalline structure of UN.

LCAO and PW Calculations on UN Bulk

Previous LCAO calculations clearly demonstrated that the chemical bonding in UN crystal has a metallic-covalent character.[13,17] The partly covalent bonds are formed by the interaction of U5*f* and 6*d* states with the N2*p* states. It was shown that the inclusion of 5*f* electrons in the atomic core (RECP81[13]) introduces small changes in the calculated cohesive energy of UN crystal and electron charge distribution. However, the inclusion of 5*s*, 5*p*, and 5*d* electrons in the valence shell results in a better agreement with values of both calculated and experimentally measured cohesion energy.

In the present and former[13] LCAO studies of UN bulk, we have used the two computer codes: the GAUSSIAN-03[27] and the CRYSTAL-06[28] suited for periodic systems. Both these codes give close results if the direct lattice summation is made up to 50 a.u. in the GAUSSIAN-03 and the tolerances 8 8 8 16 are used in CRYSTAL-06 for the Coulomb and exchange integrals calculations. The Monkhorst-Pack scheme[29] for 16 × 16 × 16 *k*-point mesh in the BZ was applied in both cases. For the N atom, the all-electron basis set 6-311++G(2*d*,2*p*)[30] was used, while the diffuse Gaussian function with the orbital exponent 0.0639 $a.u^{-1}$ was removed from the crystal calculation. As to BS of U atom, all diffuse orbitals (with orbital exponents less than 0.1 $a.u^{-1}$) were removed from the bulk calculations but retained in the free atom calculations.

The results of DFT-LCAO calculations on UN bulk using PW91 exchange and correlation functionals are presented in Table 3 for three different RECPs described above in RECP Formalism. Table 3 shows that the E_c is essentially underestimated in MT78 calculations, but is close to the experimental value in MT60 and SC60 calculations. As to the lattice parameter a_0, our LCAO DFT values (4.78 and 4.80 Å) do not differ much from those obtained in other DFT calculations (Table 1). The bulk modulus B is underestimated in MT78 calculations and overestimated both in MT60 and SC60 calculations. The calculated effective charge of U atom in UN (Q_U) is close to 1.6 *e* for all three RECP used and comparable to 1.7 *e* found in PW PAW78 calculations[10] using the topological Bader analysis.

Table 3 shows also that the populations of 6*d* and 5*f* orbitals on U atom are sensitive to the RECP choice. The AO populations allow us to analyze a role of different U atomic orbitals in the U-N chemical bonding using the RECP SC60 for a valence configuration $5s^25p^65d^{10}6s^26p^66d^15f^37s^2$. The conclusion could be drawn from the Table 3 that the sum of 5*s* and 6*s* orbital populations is close to 4 *e* thus demonstrating their small participation in the U-N chemical bonding. From the UPS and XPS investigations of the core and valence levels of UN, the popula-

Table 3. The Results of Current LCAO Calculations for UN Bulk.

Property		MT78	MT60	SC60
a_0 (4.89)		5.17	4.78	4.80
E_{tot}		−106.5218	−531.0228	−531.9898
E_U		−51.5970	−475.9572	−476.9186
E_c (13.6)		9.6	13.4	13.6
B (194)		167.2	291.6	276.9
Q_U		1.63	1.55	1.58
SD		3.18	1.18	1.06
Populations, *e*				
U	*s*	2.05	4.20	4.04
	p	5.98	12.03	12.15
	d	1.11	11.96	11.96
	f	3.23	2.26	2.27
N	*s*	3.89	3.87	3.87
	p	4.72	4.58	4.64
	d	0.02	0.10	0.07

The energy *per* unit cell E_{tot} and the U atom energy E_U (given in a.u.), the cohesive energy E_c (eV), the lattice constant a_0 (Å), and the bulk modulus *B* (GPa). The experimental values are given in brackets in the first column. The U atom spin density (SD) is given in μ_B.

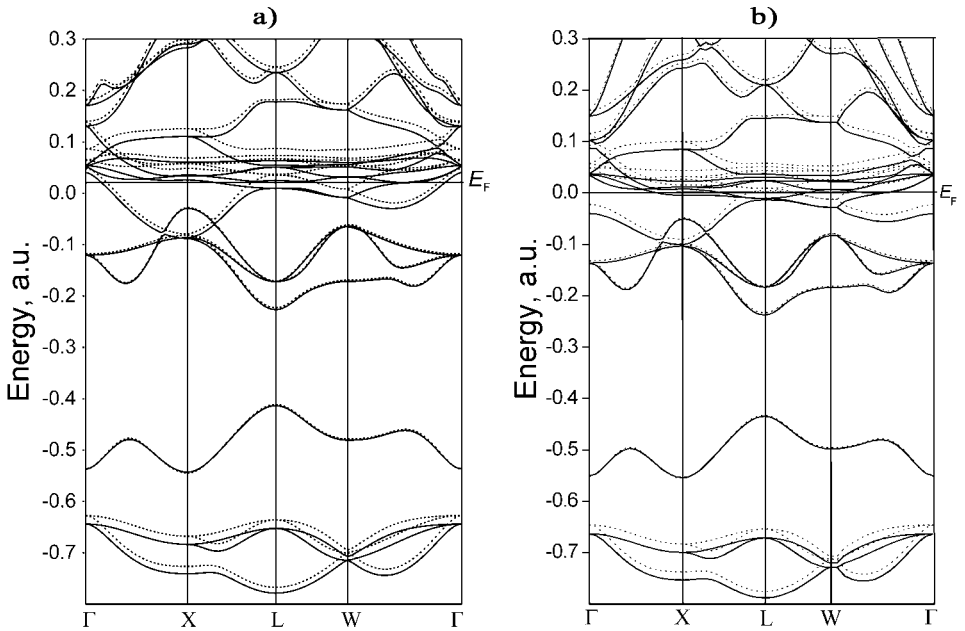

Figure 1. The energy bands of UN crystal constructed for: (a) LCAO PW91 (RECP 60) and (b) PW PW91 (RECP 78) Hamiltonians. The energies are given in a.u., solid and dotted lines correspond to the states with spin up and spin down, respectively.

tion of 2.2 ± 0.5 *e* in the U5*f* band near the Fermi level has been estimated.[17] This result is in good agreement with our DFT-LCAO (2.27 *e*, see Table 3) and FP LAPW (2.17 *e* [6]) values for U5*f* populations. As to U6*d* orbitals, their participation in the chemical bonding is seen from Table 3: for the RECP MT78, 6*d* population is 1.11 *e*, but for both RECPs-60 it is 1.96 *e*. It is also seen that the covalent part of bonding is defined mainly by N2*p* orbitals.

As follows from Table 3, the SD value in the ground state of metallic UN crystals is close to unity in the calculations with the RECP 60. The calculated spin-density of 1.06 μ_B (SC60) is the most close to the experimental value of 0.75 μ_B.[1] This result differs from that found in article[11,13] for different RECP 78 when the ground state with the spin projection 3/2 appeared to be more favorable (the three U5*f* electrons with parallel spins occupying the t_{2u} states near the Fermi level).

Figure 1a shows the upper part of the valence and the lower part of the conduction energy bands obtained in the LCAO DFT-PW91 calculations with the RECP SC60 for the total spin projection $S_z = 1/2$. The lowest in energy threefold degenerates subband and next nondegenerate subband are formed by U6*p* and U6*s*+N2*s* states, respectively. The next threefold subband centered at −0.10 a.u is formed by the hybridized U5*f* + N2*p* states. The highest subbands up to the Fermi level are formed mainly by U5*f* states. The more detailed analysis of the crystalline orbitals at the BZ shows, in particular, that the nondegenerate a_{2u} level is occupied by two (spin-up and spin-down) 5*f* electrons; the third 5*f* unpaired spin-up electron occupies three-fold degenerate t_{2g} level formed by U6*d* states. The relative position of different U5*f* subbands near the Fermi level depends on the RECP chosen. As it follows from ref. [13], the RECP78 calculations change the order of bands in such a way that three spin-up electrons occupy the states of three-fold band near the Fermi level. Thus, the spin density calculated depends on the RECP chosen (∼3 *e* for RECP78 and ∼1 *e* for the RECP60, see Table 3). The choice of the RECP SC60 is preferable, as it gives the best agreement with the experimentally known UN properties. Therefore, in our LCAO surface calculations to be analyzed in next section we used the RECP SC60 for the core electrons.

Computational procedure of the VASP code[25] used for our current DFT-PW calculations applies a standard iterative solution of the Kohn-Sham equations based on residuum-minimization and optimized charge-density mixing routines.[31] They include the calculations of the Hellmann-Feynman forces acting on the atoms and the stresses on the unit cell.[32] The total energy is optimized with respect to the positions of the atoms within the unit cell or supercell. For UN bulk PW calculations, we have applied the same 16 × 16 × 16 *k*-point mesh in the BZ in the framework of Monkhorst-Pack scheme[29] as used in LCAO calculations described above. The cut-off energy was chosen to be 520 eV for the PW91 and PBE Hamiltonians compared here. Main results of these calculations are presented in Table 4 and Figure 1b.

The conclusion could be drawn from the Table 4 that the two DFT functionals used give similar results close to the previous VASP calculations[10,11] performed with a smaller *k*-point mesh and the cut-off energy. A comparison of Tables 3 and 4 demonstrates a qualitative correlation of properties calculated using the LCAO (RECP 60) and the PW (RECP 78) methods, except for bulk modulus which is noticeably overestimated in the CRYSTAL calculations as compared with the experimental value.

The analysis of band structures for UN bulk presented in Figure 1 calculated by LCAO and PW methods using the same

Table 4. The Results of Current PW Calculations for UN Bulk and Their Comparison with Previously Published Data.

Property	PW91	PBE	PW91-PAW[10]	PBE-AE-LAPW[5,6]
a_0 (4.886)	4.868	4.867	4.864	4.886
E_c (13.6)	14.79	14.57	14.7	13.4
B (194)	227	224	226	209
Q_U	1.69	1.69	1.61	–
SD	1.15	1.19	1.05	1.25

See Table 3 footnote for explanation.

PW91 Hamiltonian demonstrates even good quantitative correlation in details especially below the Fermi level, in agreement with the experiment[7] and the previous DOS analysis performed in earlier PW VASP calculations.[11]

DFT LCAO and PW Calculations on UN(001) Surface

Single (2D) and Repeated (3D) Slab Models of a Surface

The single (2D) and repeated (3D) slab models are used in LCAO and PW surface calculations, respectively.[15] The LCAO calculations do not require artificial repeating of slab along the normal to the surface direction as it is made in PW calculations to restore 3D periodicity. However, use of atom-centered Gaussian BS faces in LCAO calculations a rather serious problem known as the basis-set superposition error (BSSE). The problem is that in a system comprising interacting fragments A and B, the fact that the basis sets on A and B are practically always incomplete means that the fragment energy of A has necessarily to be improved by the basis functions on B, irrespective there is any genuine binding interaction in the AB system or not. The improvement in the fragment energies lowers the energy of the combined AB system. The BSSE is an ever-present phenomenon and accurate calculations should always include the BSSE analysis. The examples when one should be particularly concerned include the binding energy of molecules adsorbed on surfaces or calculation of defect formation energies.[15] The approach most commonly used to estimate the BSSE effect is the *counterpoise correction*[33]: the separated fragment energies are computed not in the individual fragment basis sets, but the total basis set for the system including "ghost basis functions" for the fragment that is not present. These energies are then used to define the counterpoise-corrected (CPC) interaction energy.

In the bulk crystal the AO basis of a given atom is extended by AOs centered on atoms in the neighboring unit cells. However, in the slab calculations this is not true for surface atoms. This may lead to underestimate of the slab energy and as a consequence, to overestimate of the surface energy. Moreover, the AO used in the crystal and slab calculation may not be sufficiently diffused to reproduce correctly the electronic density distribution tail in the vacuum outside the surface. Corresponding corrections are similar to those arising for bulk solids and molecules. The simple and physically reasonable way to introduce the CPC interaction for the slab model of a surface (bare, reduced, relaxed) was suggested in ref. [34] and includes the addition of one and two extra layers of ghost atoms on both slab surfaces. The fixed ghost atoms are placed at their bulk positions, thus forming the crystallographic planes next to the surface atomic planes. The additional Gaussians are centered on the ghost atoms and called the extra layer basis set (ELBS). This approach was applied in ref. 34 in a study of water adsorption on $SrTiO_3$ (001) surface. The geometric structure of slabs was reoptimized, fixing the positions of the ghost atoms. It was found that addition of the first ELBS introduces noticeable changes in the calculated properties, whereas the second ELBS has no further effect. In particular, the BSSE correction reduces the surface energy of cubic semiconducting perovskites and decreases the water adsorption energy. For metallic UN crystal the large electron delocalization may increase the influence of the BSSE on the calculated surface energies and surface relaxation. This is demonstrated in the following section.

For DFT-PW surface calculations, we use 3D symmetric slabs consisting of 3–11 atomic layers separated by vacuum gaps up to 15 empty layers (see Fig. 2). This inter-slab distance is large enough to exclude interaction between the neighboring 2D slabs and to allow one the comparison of 2D LCAO and 3D PW results.

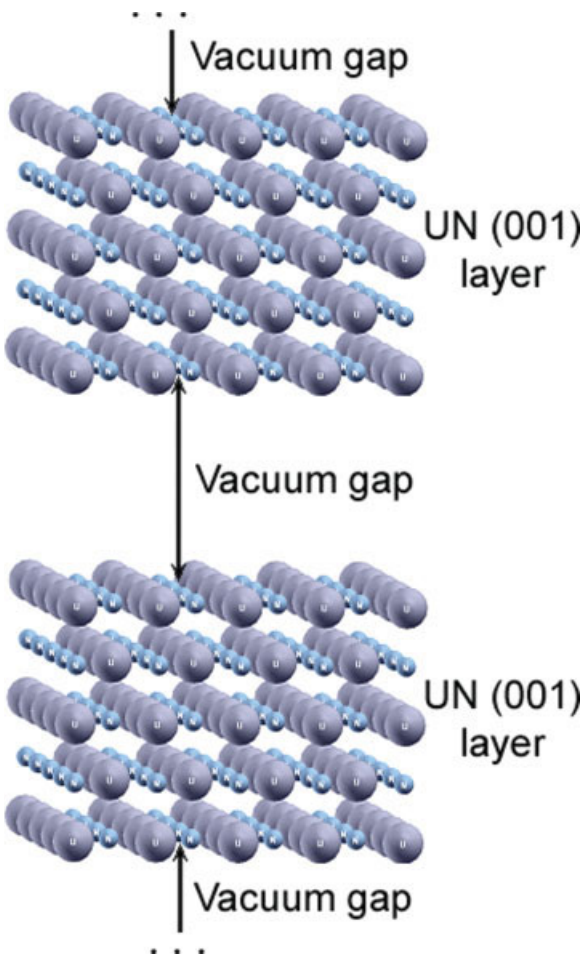

Figure 2. Side view of five-layer 3D slab model of the UN(001) surface.

Table 5. The Calculated Atomic Displacements Δz (Å) on UN (001) obtained for Different Slabs and Methods.

Atom	Method	Number of atomic planes in slab				
		3	5	7	9	11
Surface U	LCAO	−0.085	−0.095	–	–	–
	LCAO (extra layer added)	−0.026	−0.046	–	–	–
	PW PW91	−0.041	−0.020	−0.050	−0.061	−0.057
Subsurface U	LCAO		−0.011	–	–	–
	LCAO (extra layer added)		−0.001	–	–	–
	PW PW91		−0.018	−0.016	−0.013	−0.013
Surface N	LCAO	0.064	0.058	–	–	–
	LCAO (extra layer added)	0.049	0.048	–	–	–
	PW PW91	0.030	0.022	0.025	0.033	0.026
Subsurface N	LCAO		−0.002	–	–	–
	LCAO (extra layer added)		0.027	–	–	–
	PW PW91		0.026	0.028	0.032	0.022

Positive sign means an outward displacement from the slab center and *vice versa*.

In the PW surface calculations, we have used the PW91 Hamiltonian only, since a comparison between results of the PW91 and PBE calculations on UN bulk (Table 4) do not show any noticeable differences. We have applied the same Monkhorst-Pack scheme for the 8 × 8×1 *k*-point mesh. The cut-off energy was chosen 520 eV, similar to the bulk. All calculations were performed for the spin-polarized (FM) surface states.

Comparison of LCAO and PW Results for Unrelaxed and Relaxed Surface

We have analyzed in detail the vertical displacements along the *z* axis of both surface and subsurface atoms from their host lattice sites in UN bulk (Table 5), effective atomic charges (Table 6), the surface energies (Table 7) as well as DOS obtained in the PW calculations (see Fig. 3). The surface energy of an *n*-layer slab was estimated from the standard basic relationship:

$$E_{surf}(n) = \frac{1}{2S}(E_n - nE_b) \quad (2)$$

where E_n is the total slab energy per primitive surface unit cell and S its area, while E_b is the total energy per primitive bulk unit cell.

There is a good qualitative agreement between structural relaxations and effective atomic charges for the LCAO with the

Table 6. The Effective Atomic Charges $q(e)$ on the UN (001) Slab.

Atom	Method	Number of atomic planes in slab				
		3	5	7	9	11
Surface U	LCAO	1.63	1.63	–	–	–
	LCAO (extra layer added)	1.64	1.64	–	–	–
	PW PW91	1.65	1.66	1.72	1.67	1.65
Subsurface U	LCAO	–	1.51	–	–	–
	LCAO (extra layer added)	–	1.55	–	–	–
	PW PW91	–	1.65	1.63	1.63	1.69
Middle U (mirror plane of slab)	LCAO	1.45	1.57	–	–	–
	LCAO (extra layer added)	1.52	1.55	–	–	–
	PW PW91	1.62	1.67	1.72	1.65	1.62
Surface N	LCAO	−1.55	−1.55	–	–	–
	LCAO (extra layer added)	−1.61	−1.60	–	–	–
	PW PW91	−1.64	−1.63	−1.64	−1.63	−1.67
Subsurface N	LCAO	–	−1.59	–	–	–
	LCAO (extra layer added)	–	−1.57	–	–	–
	PW PW91	–	−1.67	−1.7	−1.64	−1.7
Middle N (mirror plane of slab)	LCAO	−1.61	−1.58	–	–	–
	LCAO (extra layer added)	−1.58	−1.57	–	–	–
	PW PW91	−1.65	−1.7	−1.66	−1.62	−1.64

Table 7. Surface Energies E_{surf} (J m^{-2}) and Relaxation Energies E_{rel} (eV) obtained for UN(001) Surface in LCAO and Plane Wave Calculations.

Number of atomic planes in slab			3	5	7	9	11
Method	LCAO	E_{surf} (unrelaxed)	2.20	2.29	2.28	2.11	–
		E_{surf} (relaxed)	2.06	2.13	–	–	–
		E_{rel}	0.203	0.230	–	–	–
	LCAO (extra layer added)	E_{surf} (unrelaxed)	1.68	1.45	–	–	–
		E_{surf} (relaxed)	1.430	1.38	–	–	–
		E_{rel}	0.359	0.121	–	–	–
	Plane waves PW91	E_{surf} (unrelaxed)	1.81	1.87	1.84	1.86	1.90
		E_{surf} (relaxed)	1.70	1.69	1.70	1.70	1.69
		E_{rel}	0.156	0.258	0.210	0.239	0.305

extra-layer and the corresponding PW data (Table 5). First of all, in both methods atomic displacements have the same directions: N atoms go outwards from the surface whereas U atoms relax inwards, to the slab center. This is a pattern typical for the rumpling observed on oxide surfaces but the rumpling in UN is considerably larger. One observes also substantially larger magnitudes of surface U displacements than N atoms, whereas subsurface atom relaxations are smaller.

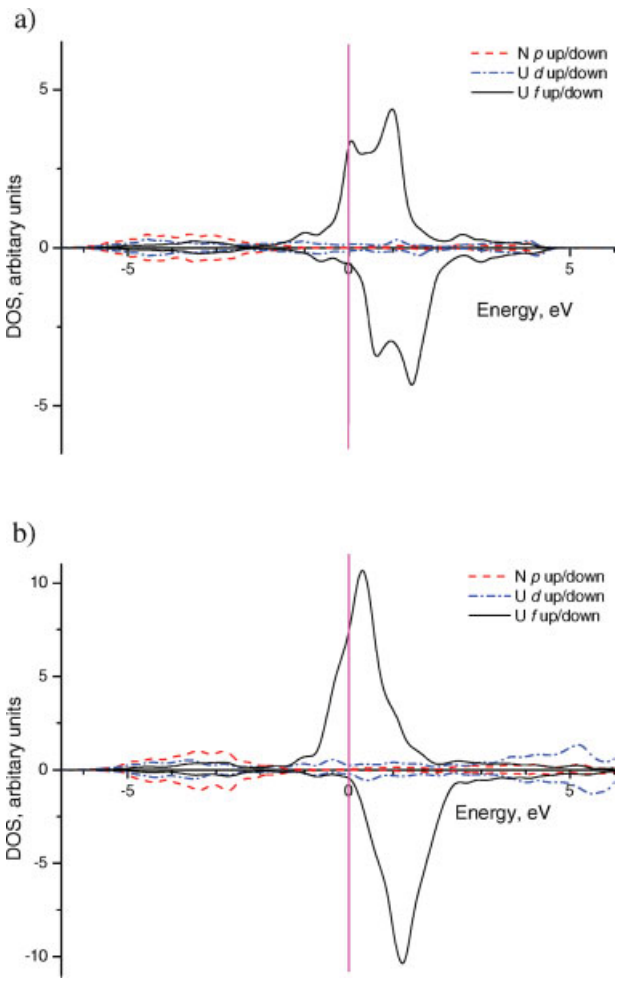

Figure 3. The projected DOS for the bulk (a) and the perfect UN(001) surface (b) in FM states.

There is also a good agreement of the effective atomic charges calculated in the LCAO and PW using two very different methods (Table 6). These charges indicate a considerable U-N bond covalency in both UN bulk and on the surface. Asymmetrical electron charge redistribution on U and N atoms is likely caused by atomic displacements from a crystalline 2D plane.

The surface energies are stabilized for slab thicknesses around 5–7 layers whereas the relaxation energy is more sensitive to the thickness (Table 7). Because of lack of experimental results, the calculated values of surface energy could be qualitatively compared only with 1.0–1.2 J/m^2 obtained recently for UO_2(001) surface energy using the quantum mechanical calculations.[2] As one can see, the surface energies of UN(001) and UO_2(001) are predicted to be similar. A qualitative agreement is observed between the UN(001) surface energies obtained in the LCAO calculations using extra-layer and the PW calculations. Increase of the number of atomic layers in the UN(001) slab stabilizes the energy of relaxed surface.

The total and projected DOS in the FM state obtained in our PW calculations is present in Figure 3. There is a small difference in band shapes from previous UN bulk calculation,[11] due to the much higher *k*-point mesh and cut-off energy used here. A comparison of the bulk DOS (Fig. 3a) with that for the projection of the surface U and N atoms (Fig. 3b) shows mainly changes in the shape of unoccupied states above the Fermi level. In both cases the mixed metallic-covalent chemical occurs with U5*f* states at the Fermi level, which is in line with previous experimental and theoretical studies[1,4–6,8].

Conclusions

In this article, we demonstrated an importance of choice of the proper effective core potentials in actinide (U) compound calculations which can considerably change the results obtained (e.g., the magnetic structure). We have also shown that the reliable LCAO calculations of the surface properties needs introduction

of an extra layer of the ghost functions simulating correct electronic density decay into vacuum from the surface. All this allowed us to perform first detailed study on properties of the densely packed UN(001) surface.

The results obtained by means of two substantially different DFT methods—LCAO and PW—demonstrate good agreement. We observed considerable relaxation of surface atoms which affects the surface energy. These results will be used in further study of surface defects and processes, first of all, UN surface oxidation which is important practical problem for its use as advanced nuclear fuel.

Acknowledgments

Authors are indebted to A. V. Titov, N. S. Mosyagin, P. Weck, A. Ray, D. Sedmidubsky, E. Heifets, Yu. Mastrikov, D. Gryaznov, and P. van Uffelen for fruitful discussions (DG, YM also for a technical assistance). D. B. gratefully acknowledges funding from the European Social Fund (ESF). This study was partly supported by the EC Framework 7 EURATOM.

References

1. Matzke, H. Science of Advanced LMFBR Fuels; North Holland: Amsterdam, 1986.
2. Skomurski, F. N.; Ewing, R. C.; Rohl, A. L.; Gale, J. D.; Becker, U. Am Mineral 2006, 91, 1761.
3. Weinberger, P.; Mallett, C. P.; Podloucky, R.; Neckel, A. J Phys C: Solid State Phys 1980, 13, 173.
4. (a) Brooks, M. S.; Glotzer, D. Phys B 1980, 102, 51; (b) Brooks, M. S. J Phys F: Met Phys 1984, 14, 639.
5. Sedmidubsky, D.; Konings, R. J. M.; Novak, P. J Nucl Mat 2005, 344, 40.
6. Atta-Fynn, R.; Ray, A. K. Phys Rev B 2007, 76, 115101.
7. Ito, T.; Kumigashira, H.; Souma, S.; Tahakashi, T.; Suzuki, T. J Magn Magn Mater 2001, 68, 226.
8. (a) Black, L.; Miserque, F.; Gouder, T.; Havela, L.; Rebizant, J.; Wastin, F. J Alloys Compd 2001, 315, 36; (b) Rafaja, D.; Havela, L.; Kuzel, R.; Wastin, F.; Colineau, E.; Gouder, T. J Alloys Compd 2005, 386, 87.
9. Yongbin, Z.; Daqiao, M.; Zhenghe, Z.; Meizhong, M. Chin J Chem Phys 2005, 18, 735.
10. Kotomin, E. A.; Mastrikov, Yu.; Zhukovskii, Yu. F.; Van Ufflen, P.; Rondinella, V. V. Phys Status Solidi C 2007, 4, 1193.
11. Kotomin, E. A.; Grimes, R. W.; Mastrikov, Yu.; Ashley, N. J. J Phys: Condens Matter 2007, 19, 106208.
12. Weck, P. F.; Kim, E.; Balakrishnan, N.; Poineau, F.; Yeamans, C. B.; Czerwinski, K. R. Chem Phys Lett 2007, 443, 82.
13. Evarestov, R. A.; Losev, M. V.; Panin, A. I.; Mosyagin, N. S.; Titov, A. V. Phys Status Solidi C 2008, 245, 114.
14. Perdew, J. P.; Wang, Y. Phys Rev B 1992, 45, 13244.
15. Evarestov, R. A. Quantum Chemistry of Solids. The LCAO First Principles Treatment of Crystals, Springer Series in Solid State Sciences, Vol. 153; Springer: Berlin, 2007.
16. Kudin, K. N.; Scuseria, G. E.; Martin, R. L. Phys Rev Lett 2002, 89, 266402.
17. Marutzky, M.; Barkow, U.; Schoenes, J.; Troc, R. J Magn Magn Mater 2006, 299, 225.
18. De Jong, W. A.; Harrison, R. J.; Nichols, J. A.; Dixon, D. A. Theor Chem Acc 2001, 107, 22.
19. Batista, E. R.; Martin, R. L.; Hay, P. J.; Peralta, J. E.; Scuseria, G. E. J Chem Phys 2004, 121, 2144.
20. Kuchle, W.; Dolg, M.; Stoll, H.; Preuss, H. J Chem Phys 1994, 100, 7535.
21. Titov, A. V.; Mosyagin, N. S. Int J Quantum Chem 1999, 71, 359.
22. Mosyagin, N. S.; Petrov, A. N.; Titov, A. V.; Tupitsyn, I. I. Progr Theor Chem Phys B 2006, 15, 229.
23. Bunday, B. D. Basic Optimization Methods; Edward Arnold: London, 1984.
24. Press, W. H.; Teukolski, S. A.; Vetterling, V. T.; Flannery, B. P. Numerical Recipes in Fortran 77: The Art of Scientific Computing; Cambridge University Press: Cambridge, 1997.
25. Kresse, G.; Hafner, J. VASP the Guide, University of Vienna, 2007. Available at: http://cms.mpi.univie.ac.at/vasp.
26. Blöchl, P. E. Phys Rev B 1994, 50, 17953.
27. Frisch, M. J.; Trucks, G. W.; Schlegel, H. B.; Scuseria, G. E.; Robb, M. A.; Cheeseman, J. R.; Montgomery, Jr., J. A.; Vreven, T.; Kudin, K. N.; Burant, J. C.; Millam, J. M.; Iyengar, S. S.; Tomasi, J.; Barone, V.; Mennucci, B.; Cossi, M.; Scalmani, G.; Rega, N.; Petersson, G. A.; Nakatsuji, H.; Hada, M.; Ehara, M.; Toyota, K.; Fukuda, R.; Hasegawa, J.; Ishida, M.; Nakajima, T.; Honda, Y.; Kitao, O.; Nakai, H.; Klene, M.; Li, X.; Knox, J. E.; Hratchian, H. P.; Cross, J. B.; Bakken, V.; Adamo, C.; Jaramillo, J.; Gomperts, R.; Stratmann, R. E.; Yazyev, O.; Austin, A. J.; Cammi, R.; Pomelli, C.; Ochterski, J. W.; Ayala, P. Y.; Morokuma, K.; Voth, G. A.; Salvador, P.; Dannenberg, J. J.; Zakrzewski, V. G.; Dapprich, S.; Daniels, A. D.; Strain, M. C.; Farkas, O.; Malick, D. K.; Rabuck, A. D.; Raghavachari, K.; Foresman, J. B.; Ortiz, J. V.; Cui, Q.; Baboul, A. G.; Clifford, S.; Cioslowski, J.; Stefanov, B. B.; Liu, G.; Liashenko, A.; Piskorz, P.; Komaromi, I.; Martin, R. L.; Fox, D. J.; Keith, T.; Al-Laham, M. A.; Peng, C. Y.; Nanayakkara, A.; Challacombe, M.; Gill, P. M. W.; Johnson, B.; Chen, W.; Wong, M. W.; Gonzalez, C.; and Pople, J. A. GAUSSIAN-03, Revision C. 02; Gaussian Inc.: Wallingford, CT, 2004. Available at: http://www.gaussian.com/.
28. Dovesi, R.; Saunders, V. R.; Roetti, C.; Orlando, R.; Zicovich-Wilson, C.M.; Pascale, F.; Civalleri, B.; Doll, K.; Harrison, N. M.; Bush, I.J.; D'Arco, Ph.; Llunell, M. CRYSTAL-06, Users Manual, University of Turin, 2006. Available at: http://www.crystal.unito.it.
29. Monkhorst, H. J.; Pack, J. D. Phys Rev B 1976, 13, 5188.
30. Available at: https://bse.pnl.gov/bse/portal.
31. (a) Kresse, G.; Furthmüller, J. J Comput Mater Sci 1996, 6, 15; (b) Kresse, G.; Furthmüller, J. Phys Rev B 1996, 54, 11169.
32. (a) Kresse, G.; Hafner, J. Phys Rev B 1993, 48, 13115; (b) Kresse, G.; Hafner, J. Phys Rev B 1994, 49, 14251.
33. Boys, S. F.; Bernardi, F. Mol Phys 1970, 19, 553.
34. Evarestov, R. A.; Bandura, A. V.; Alexandrov, V. E. Surf Sci 2007, 601, 1844.